Molecular Cell, Volume *23*

Supplemental Data

Large Conformational Changes in a Kinesin

Motor Catalyzed by Interaction with Microtubules

Keiko Hirose, Erika Akimaru, Toshihiko Akiba, Sharyn A. Endow, and Linda A. Amos

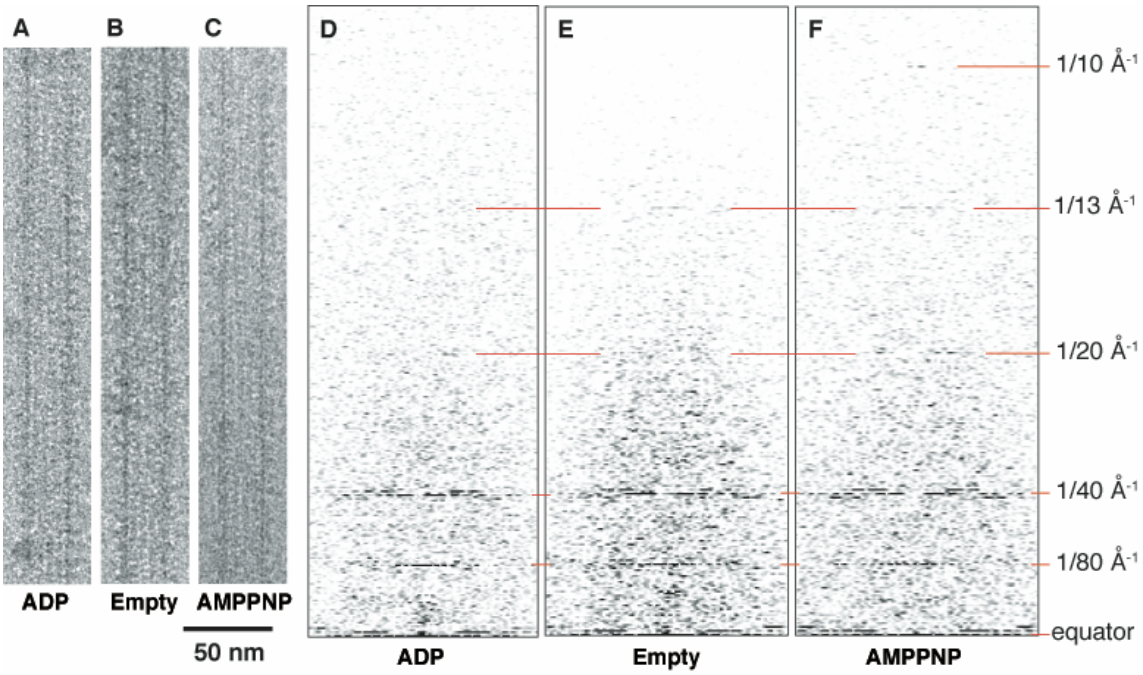

Figure S1.1. Electron Cryo-Microscope Images and Diffraction Patterns

(A-C) Images of 15-protofilament MTs decorated with the motor domain of Kar3 in the ADP (A), empty (B), and AMPPNP (C) states. The MTs we used to produce individual data sets for the final 3D maps were each ~300 nm in length, corresponding to ~560 asymmetric units with each unit consisting of one tubulin dimer + one Kar3 head. (D-F) Computed diffraction patterns from (A-C). Some of the calculated Fourier transforms showed reflections up to 1/13 $Å^{-1}$, even from a single image, and a few patterns showed a reflection at 1/10 $Å^{-1}$ (F), indicating a high level of order in the images.

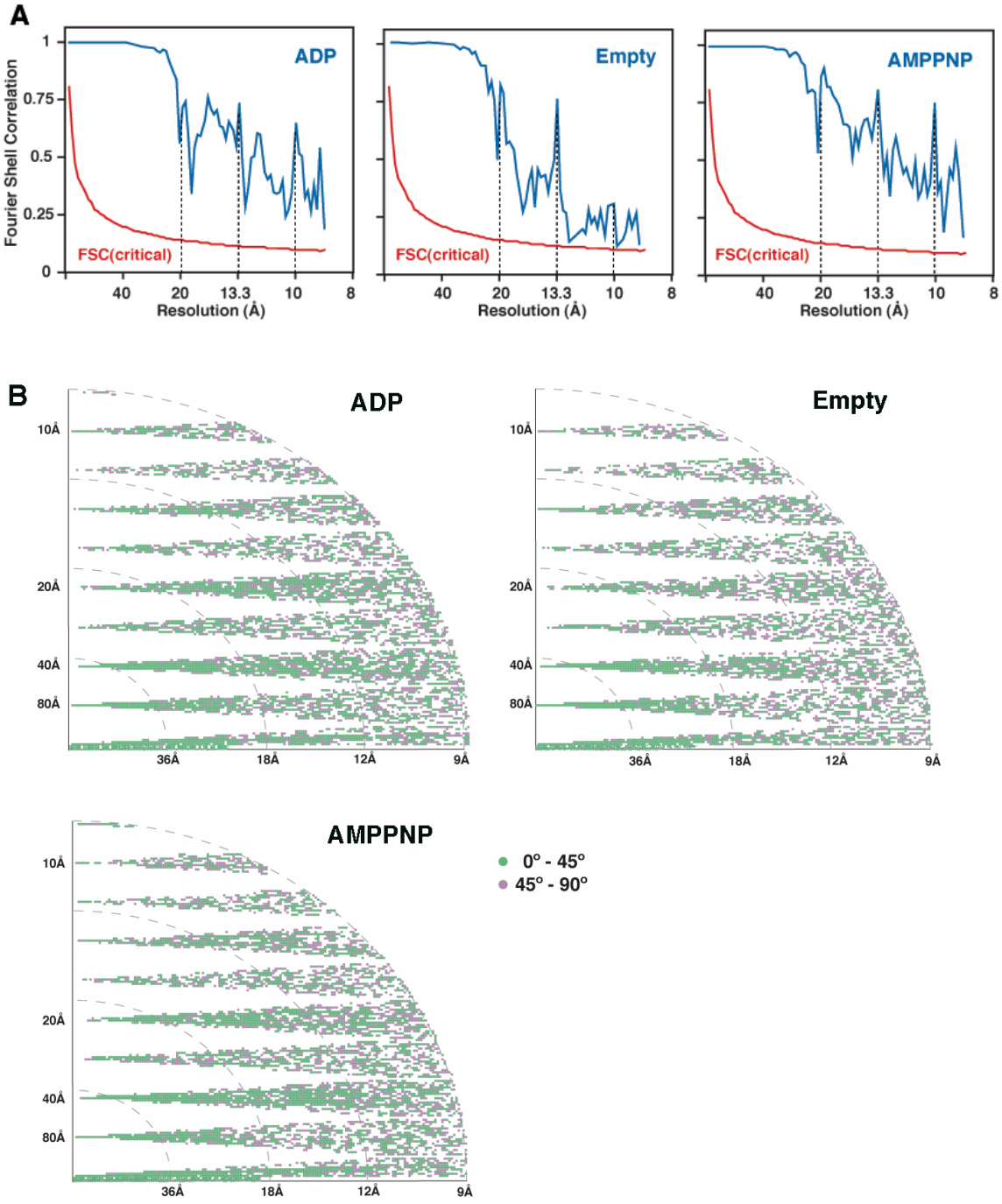

Figure S1.2. Evaluation of Resolution

To evaluate the resolution of the averaged layer-line data, Fourier Shell Correlation (FSC) values (A) were calculated from “half-averages” of the data using the RF3 function in SPIDER (Frank et al., 1996). Images of each state were divided into two groups and their

layer-line data were averaged to give pairs of independent data sets. The phase difference at each point along each layer line is indicated for each pair of data sets (B); green points show phase agreement of 0-45° and purple points 45-90° (see Kikkawa et al. (2000) for a similar figure). All of the averaged layer lines contain significant amounts of data with good phase agreement, as shown by the presence of the green points in all the layer lines down to 10 Å. This indicates good alignment of the MTs used for the Fourier transforms and well ordered data to 10 Å or lower for all three states. However, points far out along each layer line tend to disagree, showing that the resolution is not fully isotropic. Thus, the FSC curves in (A) do not drop smoothly as in data for single particle image reconstructions, because they depend on the overall correlation between the pairs of data sets within each radial shell. Peaks in the FSC curves correspond to resolution shells, indicated by dotted lines, which include parts of the layer lines that are close to the vertical axis. There are peaks higher than 0.5 extending to 13.3 Å resolution for the empty state and below 10 Å for the ADP and AMPPNP states, consistent with resolution of 10-13 Å or lower. The FSC critical values (red line) represent the expected FSC values in the absence of signal.

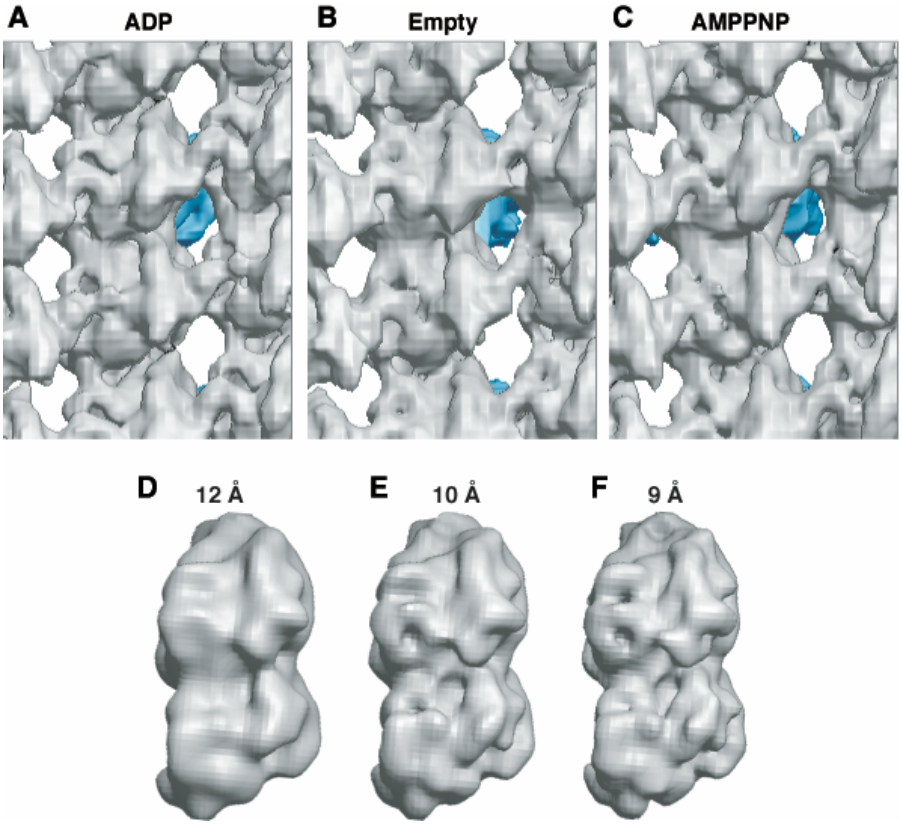

Figure S2.1. EM Maps Compared with Tubulin Atomic Structure at Lower Resolution

(A-C) Three-dimensional electron cryo-microscopy maps of the Kar3 motor (cyan) bound to MTs (grey) in the ADP (A), empty (B) and AMPPNP (C) states, viewed from the inside of the MT. (D-F) An atomic structure of tubulin (1JFF.pdb, (Löwe et al., 2001) reduced in resolution to 12 Å (D), 10 Å (E), and 9 Å (F). Comparison of the lower-resolution tubulin atomic structures with the 3D electron cryo-microscopy maps shows a close resemblance between the EM maps and the models of tubulin at 10-12 Å resolution, indicating that the resolution of our maps is approximately 12 Å or higher. The tubulin atomic structure was reduced in resolution by filtering out the higher resolution information from a Fourier transform of the pdb file.

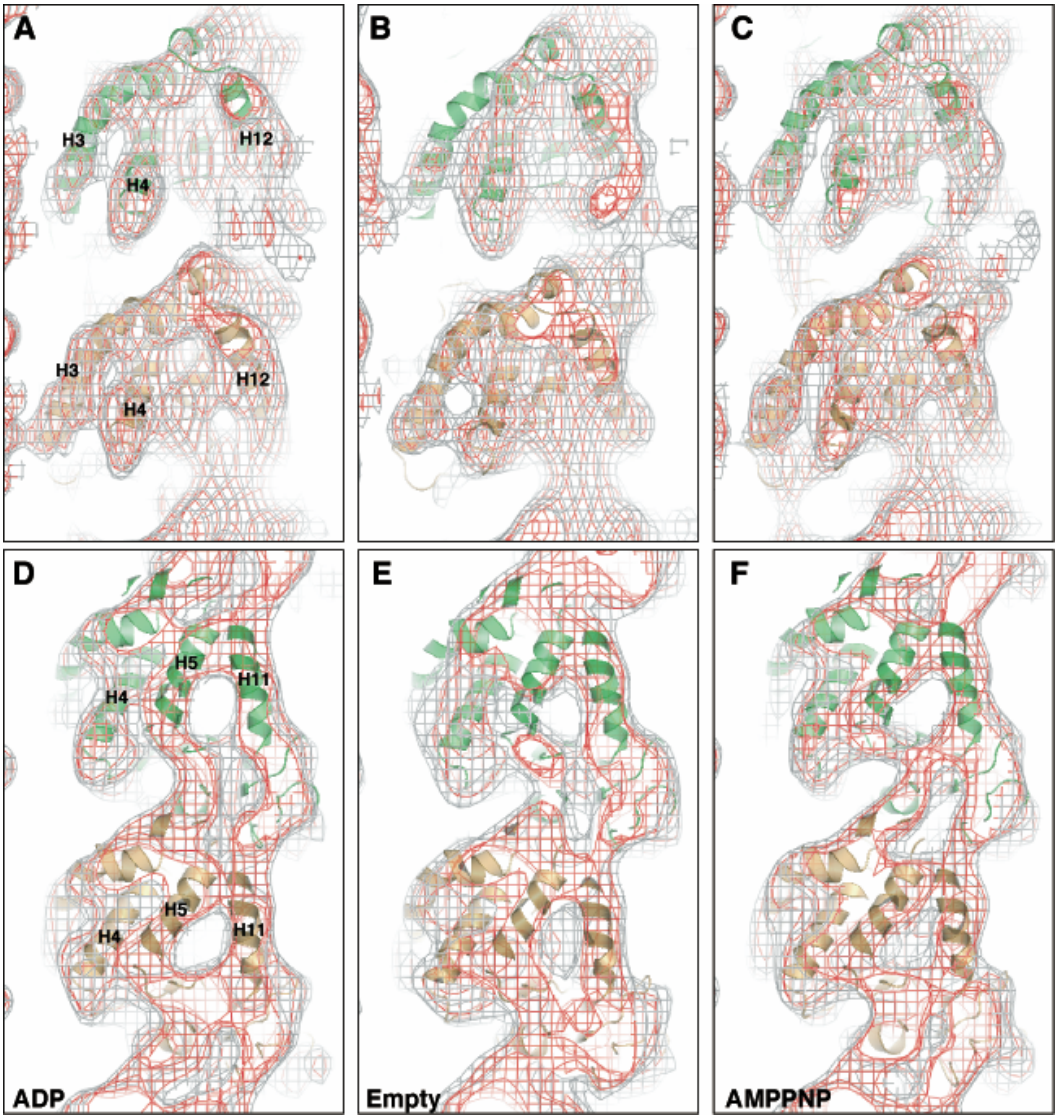

Figure S2.2. Tubulin Crystal Structure Docked into EM Maps

Longitudinal sections transecting tubulin protofilaments of the Kar3-MT complex in the ADP (A, D), empty (B, E), and AMPPNP (C, F) states. The EM maps are shown as high (red mesh) and lower (grey mesh) density, with the docked crystal structures of α-tubulin (gold) and β-tubulin (green). The maps are rotated around the MT axis by 45° (A-C) or 5° (D-F) from the front view shown in Figure 4D, with the MT plus end at the top. Most of the α-helices fit nicely into the high-density contour of the EM maps. Some of the α-helices appear as cylinders of high density.

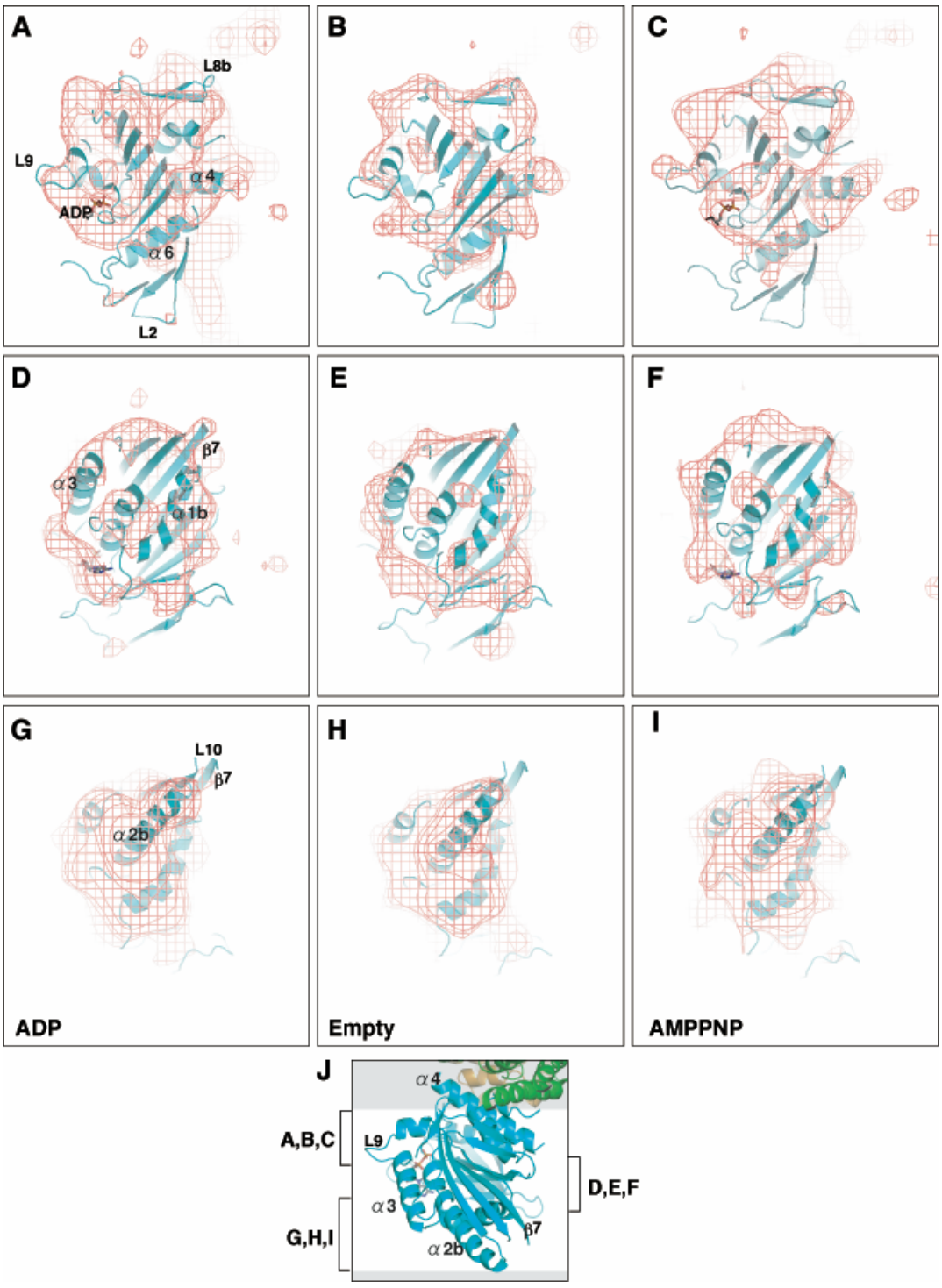

Figure S3. Kar3 Crystal Structure Fit into High Density Only in the EM Maps

(A-I) Sections at different levels of the Kar3 crystal structure docked into the high density of

the motor-MT EM maps. The sections are viewed perpendicular to the MT axis (from the outside) with the plus end at the top, sectioning tangentially to the MT surface. Sections in (A-C) are close to the MT surface, (D-F) transect the middle part of the Kar3 motor domain, and (G-I) include the most distal part of the motor domain, as indicated in (J) which shows the top view of the crystal structures with the levels of the sections. The thickness of the sections is 15 Å in (A-F), and 20 Å in (G-I). (D-I) In the empty and AMPPNP states, strand β7 extends further out of the EM density, compared to the ADP state, presumably due to the change in the central β-sheet. Otherwise, the Kar3 crystal structure shows a good fit into the high density at all three levels, with the shape of the density reflecting specific structural elements, e.g. α-helices appear as elongated cylinders of density and ends of β-strands as wedge-like projections (D), indicating that the density represents core structural elements of the motor. Structural elements that extend from the high-density regions are interpreted to show changes in conformation from the crystal structure. Changes between states in position or shape of density assigned to specific structural elements are attributed to changes in position or structure of the element. The Kar3 crystal structure fit into the EM density without detectable rotation in all three nucleotide states, in contrast to Kif1A, in which the motor core was reported to rotate clockwise by 20° in the ADP state compared with the AMPPNP state (Kikkawa et al., 2001).

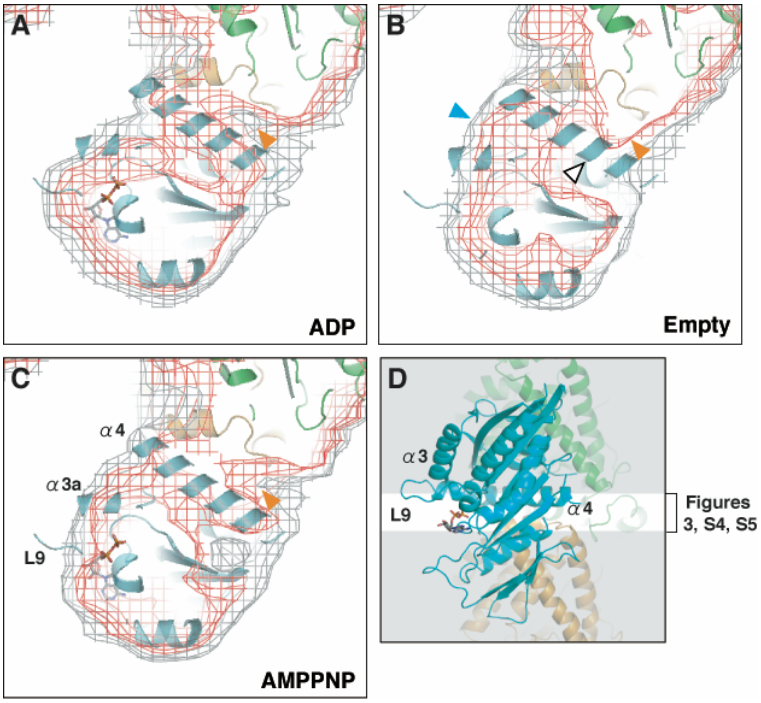

Figure S4. Unsharpened Density Maps with Docked Kar3 Crystal Structure

(A-C) Cross sections through the Kar3-MT density maps. The same sections as Figure 3 but with the Kar3 crystal structure fit into the unsharpened averaged density. The maps show changes in density corresponding to Switch I and II almost identical to those shown in Figure 3, indicating that the observed changes are not artifact produced by sharpening. (A-C) The same changes in the shape and position of density assigned to Switch I helix α3a ((B), cyan arrowhead) as observed in the sharpened density maps in Figure 3B. The ADP (A) and AMPPNP (C) maps show the same elongated cylinder of density corresponding to Switch II helix α4 as Figure 3A and C, while the empty map (B) shows the same change in shape and shift in position of the density attributed to helix α4. The end of helix α4 is no longer present in the empty state ((B), white arrowhead) and is interpreted to move to a position adjacent to tubulin (orange arrowhead). This new position of helix α4 in the empty state is lower in density in the ADP and AMPPNP states ((A) and (B), orange arrowheads). (D) Motor and tubulin crystal structures showing the level of the sections (10.7 Å thick).

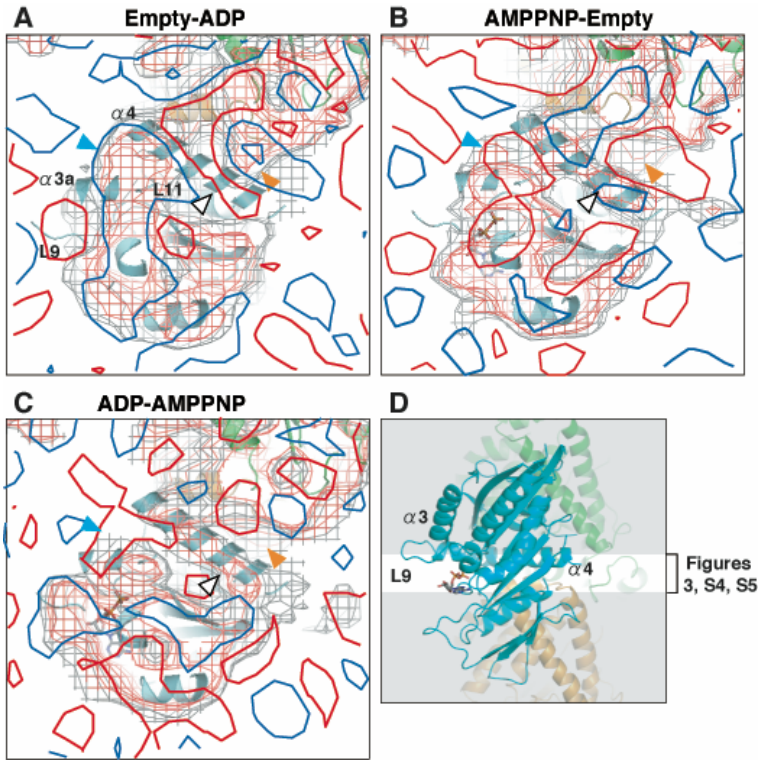

Figure S5. Difference Maps of the Kar3 Motor in the ADP, Empty, and AMPPNP States

(A-C) Cross sections through the motor-MT density maps showing density differences between the empty and ADP (A), AMPPNP and empty (B), and ADP and AMPPNP (C) maps. Density differences are positive (blue) or negative (red) with respect to the first state, but negative (blue) or positive (red) with respect to the second state. The sections are the same as Figure 3 and Supplementary Figure S4 and show the Kar3 crystal structure (cyan) docked into the density maps. Density attributed to Switch I (cyan arrowhead) increases in the empty state compared to the ADP state ((A), blue outline) and decreases in the AMPPNP states ((B), red outline). Density corresponding to Switch II helix α4 (white arrowhead) decreases in the empty state compared to the ADP state ((A), red outline) and increased density appears closer to tubulin ((A), blue outline, orange arrowhead). The cylinder of density assigned as helix α4 shows little or no change between the AMPPNP and ADP states (C). Switch I loop L9 and helix α3a of the Kar3 crystal structure are labeled in (A), together with Switch II helix α4 and the N terminus of loop L11. (D) Motor and tubulin crystal structures showing the level of the sections (10.7 Å thick).

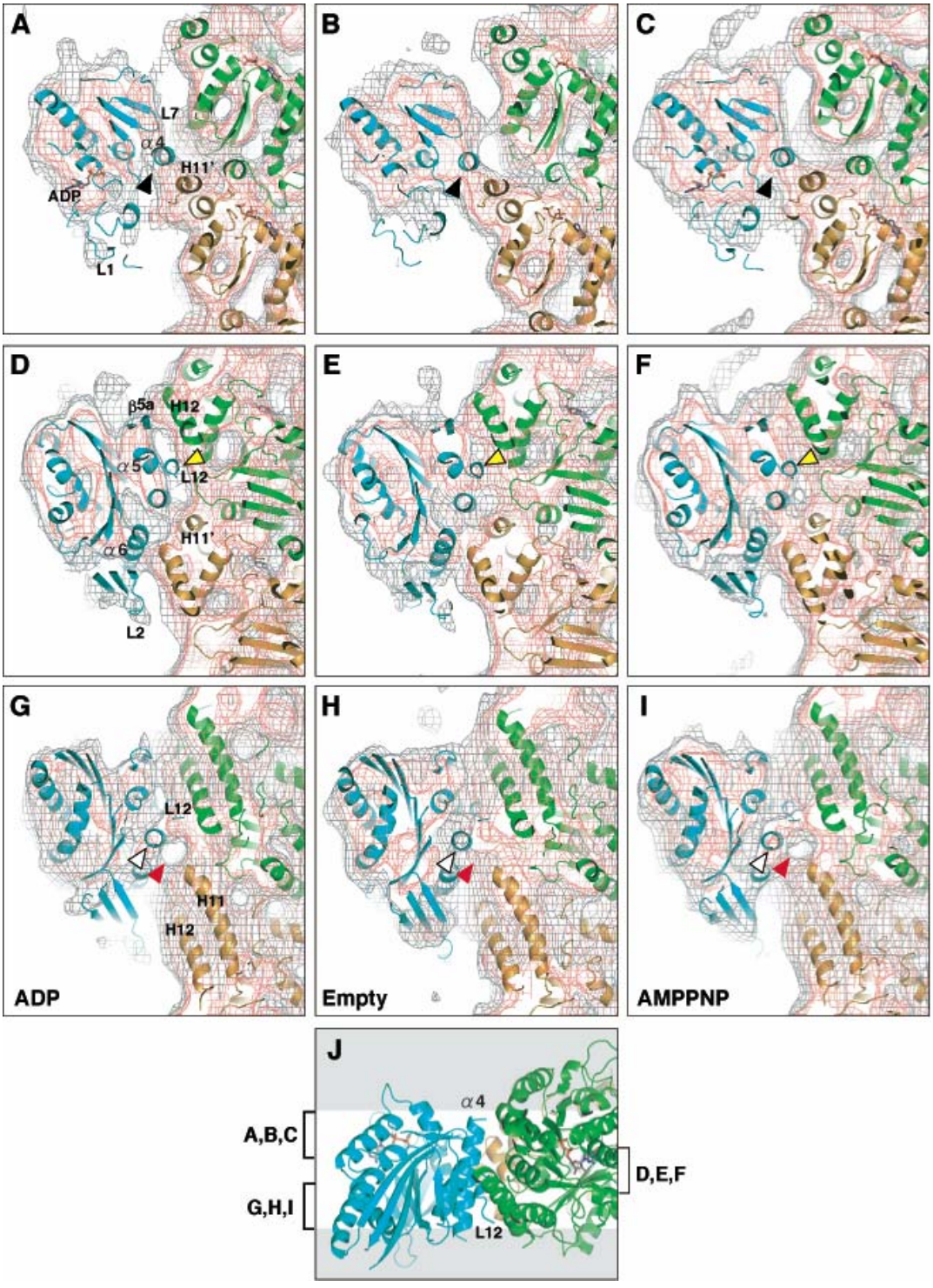

Figure S6. Changes in the Kar3-MT Interface

(A-I) Longitudinal thin sections from the same view as Figure 2, showing the Kar3-MT

interface with crystal structures of Kar3 (cyan), α-tubulin (gold) and β-tubulin (green) docked into the EM density maps. The maps are shown as high (red mesh) and lower (grey mesh) density. Sections in (A-C) include the N terminus of helix α4 (labeled in (A)), while those in (D-F) transect the middle part of helix α4 and the C terminus of loop L12. Sections in (G-I) are closer to the C terminus of helix α4. Key structural elements of Kar3 and tubulin are labeled in (A, D, G). (A-C) Density corresponding to the N terminus of Switch II helix α4 is stronger in the empty and AMPPNP states, compared to the ADP state (black arrowheads), and connected to α-tubulin (helix H11' and the H11'-H12 loop). (D- F) A contact between Kar3 helix α5 and the C-terminus of loop L12 with helix H12 of β-tubulin is strong in the empty and AMPPNP states, but absent in the ADP state (yellow arrowheads). (G-I) Density corresponding to Switch II helix α4 shifts from the ADP state (white arrowhead) to the empty state (red arrowhead), and back in the AMPPNP state. (J) Kar3 and tubulin crystal structures showing the levels at which the sections (14 Å thick) were taken.